RSC Advances

PAPER

View Article Online
View Journal | View Issue

Cite this: *RSC Adv.*, 2026, **16**, 26764

A dual crosslinked biodegradable zwitterionic chitosan–lignosulfonate derived aerogel for microbial decontamination of wastewater

Doaa Ali,[a] Samir Kamel *[b] and Naglaa Salem El-Sayed[b]

In this work, a set of novel chitosan-derived zwitterionic aerogels was synthesized *via* graft polymerization of acrylamide (Am) and 2-(*N*-3-sulfopropyl-*N*′,*N*′-dimethylammonium)ethyl methacrylate (DMAPS). The resulting copolymer aerogel underwent chemical crosslinking *via* the covalent bonds formed with *N*′,*N*′-methylenebisacrylamide (MBA), and ionic crosslinking through the electrostatic interactions between the cationic chitosan-grafted poly(DMAPS) backbone and the anionic groups of lignosulfonic acid (LSA). The morphological examination of the different aerogels by scanning electron microscopy suggested the formation of a fibrous network with varying degrees of porosity, depending on the type and amount of crosslinkers used. FT-IR, SEM, EDAX, TGA, and XRD techniques were employed to confirm the aerogel synthesis. The antimicrobial potency of the as-prepared aerogels was evaluated primarily against *E. coli*. This strain was selected as a representative Gram-negative model organism due to its high prevalence in wastewater and its relevance to environmental contamination. Preliminary investigation of the tested aerogels demonstrated that both CSH1 and CSH2 aerogels were efficient in eradicating *E. coli* from nutrient broth media at 2000 ppm after 4 h. In addition to growth-inhibition studies, the interaction between the aerogels and *E. coli* cells was examined using transmission electron microscopy and zeta potential measurements. Furthermore, the effects of aerogel dosage and contact time on antibacterial performance were systematically assessed. The results indicated that contact time is a critical factor for aerogel potency against *E. coli*. A 4 h treatment outperformed both 2 and 24 h exposures. CSH2 was selected for further evaluation using a real wastewater sample collected from a local drain. In field trials, CSH2 reduced total coliforms, fecal coliforms, *Salmonella*, and *Shigella* counts to levels deemed safe by WHO guidelines, and improved wastewater physicochemical properties. Overall, the CSH2 polymer offers a viable approach for mitigating pathogen risks in wastewater for sustainable agricultural management.

Received 7th March 2026
Accepted 4th May 2026

DOI: 10.1039/d6ra01965j

rsc.li/rsc-advances

Introduction

Water is a vital component of life, and its contamination by pathogenic microbes poses a serious threat to human health and ecosystems worldwide. Sewage farming is widely regarded as an exceptionally effective environmental strategy. However, sewage effluent contains a high load of contaminants, particularly pathogens, which accumulate in soils irrigated with sewage and can subsequently enter the food chain, causing significant adverse impacts. Globally, waterborne diseases are reported to cause more than 2.2 million deaths per year, along with a wide range of illnesses such as diarrhea, fever, and various gastrointestinal and systemic disorders. Nevertheless, many existing wastewater treatment technologies suffer from complex procedures, high costs, and secondary pollution. Treatment of sewage effluent can be achieved through one or more water remediation techniques, including chemical precipitation, adsorption, biological degradation, flocculation, ion exchange, and dialysis.[1,2] Contaminant adsorption has emerged as the most commonly employed and effective method for wastewater remediation due to its low cost, ease of operation, and reusability of the flocculants compared with other techniques.[1,3] Growing awareness of the adverse impacts of microbial contamination of water resources, which contributes to serious waterborne diseases such as dysentery, diarrhea, gastroenteritis, and nausea, has underscored the need to reduce hazardous bacterial pollutants in the environment.[4] Consequently, there is an increasing emphasis on developing rapid, eco-friendly, and affordable methods for detecting and decontaminating microbial species in wastewater. In this context, research into controlling and monitoring various pollutants using reusable adsorptive filtration scaffolds is gaining momentum.[5]

[a]*Agricultural Microbiology Department, Agricultural and Biological Research Institute, National Research Centre, Cairo, 12622, Egypt*
[b]*Cellulose and Paper Department, National Research Centre, Cairo, 12622, Egypt. E-mail: samirki@yahoo.com*

Biopolymer-based materials have gained considerable attention as eco-friendly alternatives for water purification.[6] Thousands of research papers and review articles have focused on the utilization of biodegradable biopolymers stemming from renewable and sustainable resources for the fabrication of efficient adsorbents for the treatment of wastewater.[7–12] One of these biopolymers, chitosan, a naturally derived polysaccharide obtained by deacetylation of chitin, is widely recognized for its biodegradability, biocompatibility, and intrinsic antimicrobial activity. Its cationic nature enables strong electrostatic interactions with negatively charged bacterial membranes and various organic and inorganic pollutants, making it a promising candidate for integrated water-treatment applications. These characteristics also make chitosan highly suitable for the development of pH-responsive hydrogels, flocculants, and bead-based adsorbents. Owing to this versatility, chitosan has been extensively utilized across numerous biomedical and environmental fields.[13–15] However, native chitosan suffers from inherent limitations, including low surface area, poor mechanical stability, and pronounced pH sensitivity, which collectively limit its efficiency and reliability in real wastewater treatment environments.[16] To overcome these challenges, researchers have increasingly focused on engineering chitosan-based aerogels, a class of ultra-lightweight, highly porous materials with exceptional surface area and tunable physicochemical properties.[17] Aerogel architecture enhances adsorption capacity, diffusion pathways, and structural integrity, enabling improved performance in both antimicrobial and pollutant-removal applications.[18] Crosslinking strategies, particularly those employing bio-based crosslinkers, further strengthen the mechanical stability and functional versatility of chitosan aerogels.[19–21]

On the other hand, zwitterionic aerogels are a new class of porous materials that integrate the high surface area and lightweight properties of aerogels with the antifouling and hydration-layer-forming properties of zwitterionic polymers. Their biocompatibility, resistance to protein adsorption, and adsorption properties make them promising for environmental applications. Zwitterionic aerogels derived from chitosan represent an emerging class of multifunctional materials designed to overcome the inherent limitations of native chitosan in complex wastewater environments.[22,23] By introducing both positively and negatively charged functional groups onto the chitosan backbone, the resulting zwitterionic network exhibits enhanced charge balance, improved hydration capacity, and superior resistance to fouling.[24,25] These properties significantly strengthen the aerogel's ability to interact with a wide spectrum of pollutants, including dissolved organic matter, heavy metals, dyes, and pathogenic microorganisms. When engineered into an aerogel architecture, the material gains additional advantages, ultra-high porosity, large surface area, and rapid mass-transfer pathways, making it highly effective for adsorption, flocculation, and microbial control.[26–28] Such chitosan-based zwitterionic aerogels therefore offer a sustainable, biodegradable, and tunable platform for advanced wastewater treatment, particularly in systems requiring simultaneous removal of chemical contaminants and biological hazards.[29] For example, Yang *et al.*[16,30] reported the development of a quaternary ammonium salt of carboxymethyl chitosan-graft poly[(2-methacryloyloxy)ethyl]trimethyl ammonium chloride copolymer (CMC-*g*-PDMC) for the decontamination of *Escherichia coli*. The effects of flocculant dosage, initial bacterial density, nutrient medium content, and pH on flocculation performance and bacterial viability were systematically assessed. Xiang Li *et al.*[31] grafted chitosan with methacrylamidopropyl trimethylammonium chloride (MAPTAC) acrylamide (AM) monomers under UV irradiation. The resulting copolymer, chitosan-*g*-poly(AM-*co*-MAPTAC), exhibited excellent solubility, biodegradability, effective flocculation, and potent bactericidal properties. Functionalizing hydrogels with zwitterionic molecules impart strong antifouling behavior and introduces additional chelation and interaction sites, thereby enhancing their overall performance in water-treatment and antimicrobial applications. For instance, graft copolymerization of 2-hydroxyethyl methacrylate (HEMA) and methacrylate trimethylammonium chloride (DMC) onto chitosan produced a novel comb-like chitosan-derived flocculant, CS-*g*-P(DMC-*co*-HEMA) (CPDH), characterized by improved hydration through extensive hydrogen bonding. The hydroxyl groups contributed by HEMA increase solubility and water affinity, while the quaternary ammonium groups from DMC impart potent antibacterial activity against both *Staphylococcus aureus* and *Escherichia coli*.[32] In a recent report, silver nanoparticles were *in situ* immobilized within chitosan-*g*-poly(sulfobetaine methacrylate) hydrogel beads prepared *via* graft copolymerization. These zwitterionic, nanoparticle-loaded hydrogel beads exhibited strong bactericidal activity against *Escherichia coli*, along with excellent anti-biofouling performance and notable reusability during repeated treatment cycles.[33]

The term dual crosslinking refers to the use of two distinct strategies to reinforce an aerogel network. For example, a double-cross-linked biohybrid aerogel bead (DCBA) was fabricated from waste bamboo paper and chitosan through sequential physical crosslinking (hydrogen bonding and electrostatic interactions between $-COO^-$ and $-NH_3^+$ groups) followed by chemical crosslinking (amide formation and Si–O–C condensation). For instance, Yang *et al.*[30] developed dual-network chitosan/itaconic acid aerogels with tunable ionic and covalent crosslinking using freeze-drying and controlled heat-induced amidation. Modulating the crosslinking degree significantly enhanced mechanical strength, hydrophobicity, stability, and thermal performance while preserving the antibacterial functionality.

Consequently, in the present work, chitosan-derived zwitterionic aerogels were synthesized by grafting chitosan with poly(acrylamide-*co*-sulfopropyl-*N*,*N*-dimethylammonium methacrylate) followed by dual crosslinking by ionic crosslinker using lignin sulfonic acid sodium salt, and methylenebis(acrylamide). These dual crosslinking modes produce a more robust, tunable aerogel with an improved functional performance and stability. LSA is a biomass derived, water soluble byproduct of the sulfite pulping industry and is generally regarded as a low toxicity, renewable, and biodegradable crosslinker, which aligns well with the sustainability goals of

this study. Am is a petroleum derived monomer with known neurotoxicity in its unreacted form; however, in this study, it undergoes complete polymerization into polyacrylamide, which significantly reduces its environmental risk. The new aerogels were subsequently evaluated for their ability to eradicate *Escherichia coli* and other pathogenic coliform from wastewater collected from a local drainage system. In addition, the aerogels were tested using real wastewater sample collected from a local municipal treatment facility to assess their practical applicability under real conditions.

Materials and methods

Materials

Chitosan (CS) (high molecular weight, deacetylation degree 85%, viscosity 800–2000 cp, 25 °C, Brookfield), 2-(*N*-3-sulfopropyl-*N*,*N*-dimethylammonium)ethyl methacrylate (DMAPS), *N*,*N*-methylenebisacrylamide (MBA), lignosulfonic acid (LSA) (average MW ~ 52 000), and potassium persulfate (KPS) were purchased from Sigma Aldrich. Acrylamide (Am) was purchased from Fluka. The tested indicator pathogen, *Escherichia coli* (accession number ATCC 51659), was received from the Environmental Pollution Department at the National Research Centre. Tryptic Soy Broth (TSB), Nutrient Broth (NB), and agar media were prepared according to the method described by Atlas *et al.*[34] All selective media were purchased from HiMedia Company, India.

Graft polymerization and crosslinking of DAMPS and Am into chitosan

CS underwent surface functionalization *via* the graft polymerization of DMAPS and Am, as described previously,[9,27] with some modifications. In a typical preparation procedure, 4 g of CS was suspended in 200 mL of distilled water under magnetic stirring at 550 rpm, and 4 mL of HCl (36%) was added to the CS suspension. The stirring was continued overnight at room temperature until a clear homogeneous solution was obtained. After complete dissolving, the pH of the CS solution was carefully adjusted to 4.5–5 by adding a few drops of 10% KOH. Then, a calculated amount of KPS (0.46 mM, 0.12 g) was added to 50 mL CS solution at 65 °C under nitrogen flow. The stirring was continued for 10 min to allow the formation of free radicals. An aqueous mixture containing Am (56.27 mM, 4 g) and DMAPS (9.7 mM, 2 g) was neutralized by 10% KOH solution and added to the CS solution while stirring. The pH of the reaction mixture was readjusted to 5.5. After 10 min, an aqueous solution of the appropriate crosslinker was added to the reaction mixture as shown in Table 1, while maintaining the pH of the entire mixture at 5.5, and the temperature was set to 70 °C with magnetic stirring for an additional 2 h. The resulting aerogel was washed with distilled water (250 mL × 3) and boiling acetone (250 mL × 3) to remove the water-soluble unreacted monomers, crosslinker, and homopolymers. Finally, the samples were coded CSH1, CSH2, CSH3, and CSH4 and freeze-dried.

Table 1 Aerogel code

Crosslinker	N/A	LSA	LSA	MBA
Mg	0	250	500	250
Aerogel code	CSH1	CSH2	CSH3	CSH4

Structure characterization

The FT-IR spectra for pristine CS, CSH1, CSH2, and CSH4 were determined by a Nicolet Impact-400 FT-IR spectrophotometer in the range of 500–4000 cm^{-1}.

The XRD profiles of pristine CS, CSH1, CSH2, and CSH4 were obtained on a Diano X-ray diffractometer using a CoKα radiation source at 45 kV ($\lambda = 0.15418$ nm) over a 2θ range of 0°–80°.

The spatial elemental distribution of pristine CS and CSH1, CSH2, and CSH4 aerogels was studied using a non-destructive energy-dispersive X-ray (EDX) unit attached to a scanning electron microscope (JSM 6360LV, JEOL/Noran).

For surface morphology examination (SEM), the selected samples were recorded using an accelerating voltage of 10–15 kV. The thermal stability of CS, CSH1, CSH2, and CSH4 were tested by thermogravimetric analysis (TGA) using a STA 6000 PerkinElmer Analyzer from 25 to 800 °C at a heating rate of 10 °C min^{-1} under nitrogen.

The high-resolution transmission electron microscope investigation (HRTEM) was performed using a JEOL JEM-2100 at an acceleration voltage of 120 kV.

The zeta potential measurements for the prepared samples were performed using Particle Sizing Systems, Inc., Santa Barbara, Calif., USA. The analysis was carried out at a scattering angle of 90° and a temperature of 30 °C. The samples were measured in triplicate, and the reported values are the mean diameter ± SD.

Antibacterial assay

Preparation of culture media for *E. coli*. *E. coli* was enriched using Tryptic Soy Broth (TSB) as described by the American Public Health Association (APHA, 2005), and a single strain was isolated by streaking on nutrient Agar. This strain was inoculated into a flask containing TSB and incubated at 37 °C for 24 h. The inoculum was then suspended in TSB media containing 20% glycerol and frozen at −80 °C. A working culture was kept on a nutrient agar slant.

Effect of aerogel structure and concentration on *E. coli* enumerations. The tested aerogels were added to pathogenic *E. coli* culture (ATCC 51659) at a series of concentrations (0, 500, 1000, 1500, 2000, 3000, and 4000 ppm). To assess the effect of the as-prepared aerogels on *E. coli* eradication, a series of experiments was conducted in Nutrient Broth (NB). Briefly, an overnight culture of *E. coli* was incubated in 50 mL of NB at 37 ± 0.50 °C. Subsequently, different 50 mL flasks were charged with 49 mL of freshly prepared NB media, and 200 μL of the overnight *E. coli* culture (optical density = 0.2) was added to each flask. Varying concentrations of the tested samples (0, 500, 1000, 1500, 2000, 3000, and 4000 ppm) were added to each flask with gentle shaking. The flasks were then incubated at 37 ± 0.5 °C on an orbital shaker for different times (0, 2, 4, and 24 h).

Subsequently, 1 mL of each sample at each time interval was removed from the incubation flask and diluted with 9 mL of dilution blank to achieve a 10^{-2} dilution of the original sample. The following dilutions were prepared as needed, up to 10^{-8}. The diluted samples were analyzed using the plate count method. All antimicrobial assays were performed in triplicate.

Elucidation of the inhibition mechanisms of CSH1 and CSH2 by *E. coli* enumeration analysis. Further experiments were performed to elucidate the mechanisms by which the CSH1 and CSH2 aerogels reduce the density of *E. coli* in NB medium. 50 mL flasks containing NB supplemented with 2000 ppm of either CSH1 or CSH2 were inoculated with *E. coli* at an initial optical density of 0.2 and incubated for 4 h. After incubation, samples were withdrawn from each flask for enumeration, and then these flasks subjected to vigorous mixing for 5 min under magnetic stirring at 1000 rpm to ensure uniform dispersion of cells and aerogel particles. A second set of samples was collected immediately after mixing and used to enumerate *E. coli* to assess the impact of aerogel treatment on bacterial viability.

Elucidation of the inhibition mechanism by transmission electron microscopy (TEM). The mechanism of interaction between *E. coli* and CSH1 or CSH2 aerogel was further investigated by TEM following the method described by Liu *et al.*[35] In brief, 400 μL of an overnight *E. coli* culture was inoculated into 9.6 mL of reverse osmosis-purified water, with or without 500 ppm of CSH1 or CSH2 aerogel. The prepared suspensions were incubated at 37 ± 0.5 °C for 4 h, then observed by TEM.

Evaluation of CSH2 for wastewater decontamination. A wastewater sample was collected from the surface of Belbies drain (Sharqia governorate, Egypt) at a depth of 0–30 cm. The wastewater sample is a mixture of agricultural drainage water and sewage effluent. The wastewater sample was subjected to microbiological analyses according to Atlas 2005 and Merck for Manual Microbiology 12th Edition, 2010.[36] The serial dilution technique was used to enumerate pathogenic bacteria on selective media, and results were determined by the reaction observed after full colony growth (CFU).

The assessment of various physico–chemical parameters of wastewater samples, including temperature, turbidity, biological oxygen demand (BOD), chemical oxygen demand (COD), and total organic carbon (TOC), was carried out according to the reported methods.[37,38] Total coliforms and faecal coliforms were enumerated onto MacConkey agar media and incubated at 37 and 44 °C for 24 and 48 h, respectively. *Salmonella* and *Shigella* were enumerated onto *Salmonella–Shigella* media incubated at 37 °C for 48 h and identified by culture, morphological characters, and biochemical reactions according to the scheme illustrated by Quinn *et al.*[39]

CSH2 was evaluated for its ability to decontaminate the test pathogens in the wastewater sample. 200 mL of the wastewater sample was placed in flasks. Varying concentrations of CSH2 (0, 1000, 2000, 3000, and 4000 ppm) were added to each flask, which were then gently mixed for 4 h. An initial sample was taken at 0 time before incubation. Then, the following samples were taken after 4 h of incubation. One milliliter of each sample at each time interval was added to a 9 mL dilution blank, resulting in a final dilution of 10^{-2} of the original sample. Subsequent dilutions were prepared as needed, up to 10^{-8}. The dilutions were analyzed for tested pathogens using the plate count method.

Results and discussion

Rational design for the scaffolds

Zwitterionic composites have demonstrated significant potential to enhance antibiofouling performance and ensure compatibility among polymer matrices, organic, and inorganic composite components. In this context, sulfobetaine methacrylate serves as a prime example of a zwitterionic compound, as it contains both a positively charged quaternary ammonium group and a negatively charged sulfonate group within a single monomer. This dual functionality enables the composite to respond to a wide range of external stimuli, while the quaternary ammonium group imparts strong antimicrobial potency to the aerogel. CS functionalization *via* graft polymerization of DMAPS and Am to generate a new zwitterionic flocculant CS-*g*-poly(AM-*co*-DMAPS) or CSH1, which carries strong cationic and anionic functionalities as demonstrated in Fig. 1.

Crosslinking of the resulting copolymer was achieved using two approaches. The first one was achieved through physical ionic interaction, using two different LSA weight ratios. Crosslinking occurred *via* ionic interactions between the positively charged primary and quaternary amino groups of CS copolymer chains and the negatively charged sulphonate groups of LSA, affording two aerogels (CSH2 and CSH3). The second crosslinking strategy was achieved through irreversible chemical crosslinking using MBA, affording a flocculent aerogel (CSH4), as shown in Table 1. Besides the weak hydrogen bonds between the different functionalities along the copolymer chains. LSA and MBA were selected as dual crosslinkers due to their distinct and complementary functions.

Unlike conventional aerogels prepared by single-mode covalent or ionic crosslinking, our dual crosslinking strategy integrates both permanent covalent bonds and reversible ionic interactions, enabling tunable architecture, charge distribution, and antimicrobial performance. In contrast to widely used covalent crosslinkers such as glutaraldehyde, which provide structural stability but lack intrinsic antimicrobial activity, or ionic gelation agents such as calcium ions, which offer reversible binding but limited functional contribution, LSA serves a dual role. LSA not only acts as an ionic crosslinker but also enhances decontamination efficacy through its negatively charged sulfonate groups, which form strong electrostatic interactions with the protonated $-NH_3^+$ groups of chitosan, and it also functions as a strong chelator for different water contaminants. Besides, the polyphenolic lignin backbone is well recognized for its intrinsic antimicrobial properties.[40] This multifunctionality distinguishes our approach from conventional methods and underscores the novelty of the aerogel system.[27,41] The use of MBA crosslinker that forms covalent bonds between polymer chains, generating a stable and mechanically reinforced network that preserves porosity and structural integrity.[9] Together, these two crosslinkers enable

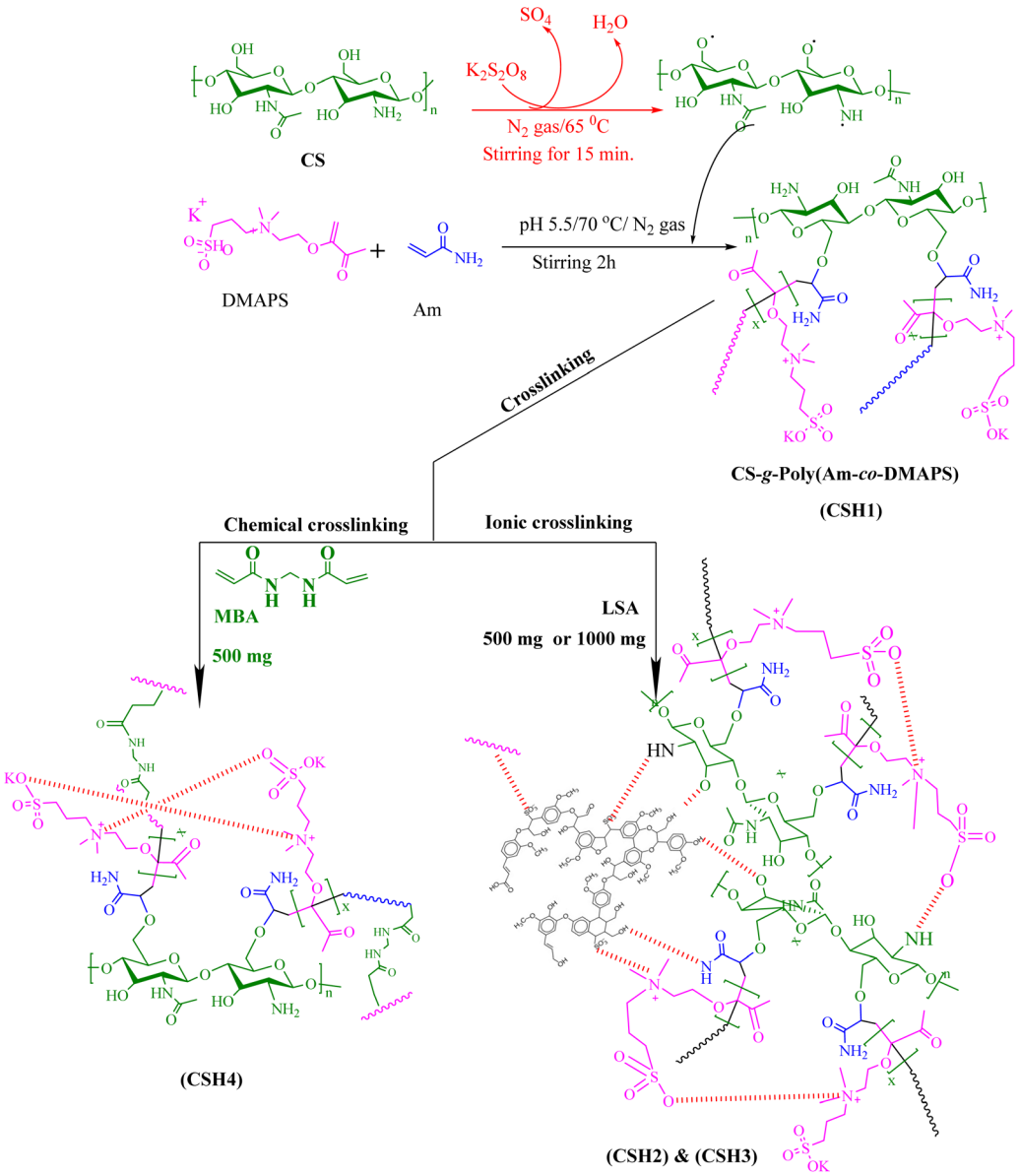

Fig. 1 Synthesis of CSH1, CSH2, CSH3, and CSH4 *via* graft polymerization of CS with Am and DMAPS with MBA or LSA as cross-linker.

simultaneous optimization of surface charge, mechanical stability, and antimicrobial efficacy.

Structure characterization

FTIR characterization. Infrared spectroscopy (IR) is one of the primary analytical techniques used to study the chemical structure and properties of CS. CS exhibits specific IR absorption bands that are directly related to its functional groups and degree of deacetylation. In the IR spectrum of CS (Fig. 2a), the typical observed bands are: the broad bands around 3373 and 3276 cm^{-1}, assigned to the stretching of O–H and the primary NH_2.[14] The C–H stretching bands in the region of 2908 and 2858 cm^{-1} often correspond to aliphatic C–H and acetyl CH_3. The critical amide bands, including the amide I at 1660 cm^{-1} and the amide II at 1592 cm^{-1}. The bands at 1591, 1423, 1317, 1269, 1153, and 1060 cm^{-1} are attributed to C–O, C–C, and C–O–C, C–NH stretching vibrations, which are present within the CS chain.[42]

The FTIR spectrum for CSH1, Fig. 2a, displayed the following bands: the broad band at 3445 cm^{-1} due to the inter and intramolecular hydrogen bonds, NH_2 of grafted polyacrylamide, and the bands at 2916 and 2884 cm^{-1} are attributed to the stretching vibration of CH, CH_2, and CH_3 groups. The bands at 1671 and 1628 cm^{-1} are assigned to the stretching vibration of the (C=O) amide I and II groups.[13] This notable shift in this band is due to the grafting of poly(Am) and poly(DMAPS) on the CS backbone. The shifting of the bending vibration bands attributed to the N–H and CH_2 groups in CS and poly(DMAPS) to 1515 and 1459 cm^{-1} is often due to scissoring. The bands at 1412 and 1384 cm^{-1} are due to the SO_3^- group from DMAPS and the CH_3 group or C–N stretching from poly(DMAPS) or

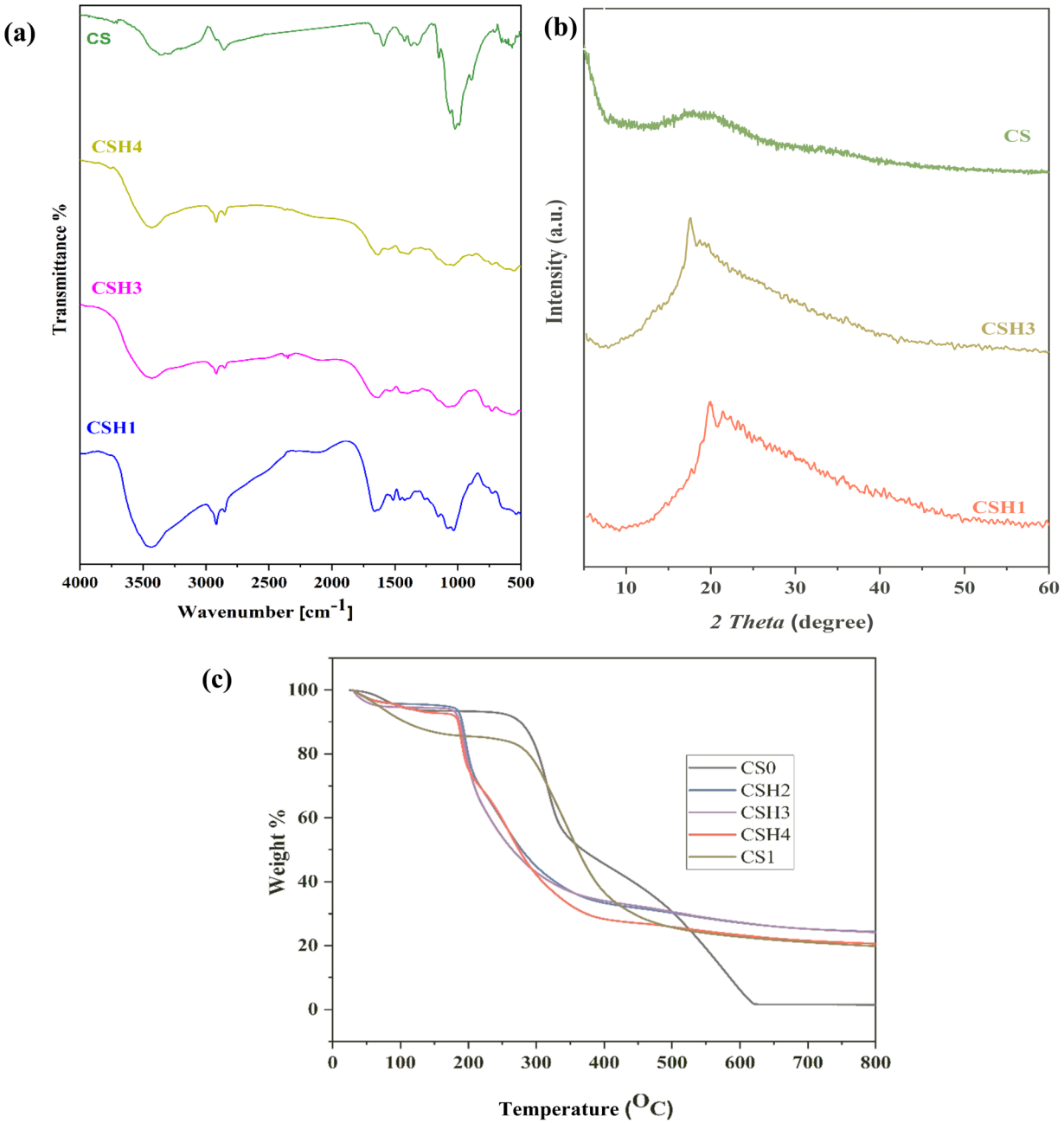

Fig. 2 (a) FTIR, (b) XRD, and TGA curves for CS, CSH1, CSH3, and CSH4.

poly(Am), respectively. Bands at 1148, 1075, and 1027 cm^{-1} are assigned to C–O–C stretching vibration, quaternary ammonium, S=O asymmetric stretching, S=O symmetric stretching of the sulfonate group, and the stretching C–O and C–N vibrations originate from alcohol, ether, and quaternary ammonium groups.[33,43] When LSA was employed as an ionic crosslinker, as in the case of CSH3, the shift in the characteristic bands to 3438, 2927, 2848, 1635, 1548, 1458, 88 1262, 1155, 1085, and 1035 cm^{-1}, confirming the grafting of MBA and the crosslinking between the polymeric chains.[27,44]

After crosslinking CSH1 chains using MBA, the FTIR spectrum for CSH4 revealed that the broad band at 3437 cm^{-1} is assigned to the hydrogen bonding and the overlapping between the alcoholic and phenolic OH groups, and the different NH bonds.[45] Also, the bands at 2927 and 2849 cm^{-1} indicate the presence of new groups, such as OCH_3 and aliphatic chains on the lignin backbone, in addition to CH, CH_2, and CH_3 groups from CS and grafted CS. Besides, the bands at 1635, 1548, and 1458 cm^{-1} are assigned to the amide I and amide II stretching vibrations of aromatic C=C, C–O, C–C, and C–O–C, C–NH stretching vibrations.[46] The shifting of characteristic bands for 1388, 1256, 1156, 1083, 1035, and 888 cm^{-1} compared to those in CSH1. These bands are attributed to C–H bending, C–N, C–O stretching, quaternary ammonium, asymmetric and S=O

symmetric stretching of the sulfonate group, and out-of-plane C–H bending.[47,48]

X-ray diffraction (XRD) patterns. Fig. 2b shows the XRD analysis, which provides insight into the structure of CS upon chemical modification with Am and DMAPS, both in grafted (CSH1) and crosslinked (CSH3) forms. The XRD patterns show that native CS is semi-crystalline, as indicated by the broad peak around $2\theta \approx 20°$ characteristic of the crystalline regions in CS, which is attributed to ordered hydrogen bonding between polymer chains.[49]

Grafting of Am and DMAPS onto CS (CSH1) alters its crystalline structure, as evidenced by a shift in the XRD peak to $2\theta \approx 19.9°$, reflecting a more ordered microstructure. This may be due to reduced steric hindrance compared to native CS. Cooperative interactions among zwitterionic and amide groups. In addition to the formation of aerogel networks after crosslinking (CSH3), a more noticeable diffraction peak is observed. This can be attributed to crosslinking, which restricted the polymer chain's movement and formed a more regular network. The sharper peak with high intensity reflects an increase in crystallinity, attributed to the synergistic effect of grafting and crosslinking. Comparing XRD patterns reveals the transition from CS (amorphous) to CSH1 (semicrystalline) to highly ordered CSH3, highlighting the effect of chemical modification on CS's structural properties. So, incorporating Am and DMAPS not only introduces functional groups but also improves the material's rigidity, and crosslinking increases this effect.

Thermogravimetric analysis (TGA). TGA delineates key decomposition stages and transitions, which are crucial for understanding the material's performance under different thermal conditions. Fig. 2c presents the TGA curves of unmodified CS and CSH1 and CSH2, CSH3, and CSH4.

For native CS, the initial weight loss (6%) at (∼50–118 °C) is due to evaporation of physically adsorbed water and loosely bound moisture. The second stage of weight loss was (47%) at a temperature range (∼250–350 °C), due to the thermal cleavage of glycosidic linkages and deacetylated units in the CS backbone. The final thermal degradation stage was the major one, occurring between 365 and 625 °C, with 97.5% cumulative weight loss and a residual ash content of only 2.5%. During this stage, the pyrolysis of carbonaceous residues and complete volatilization of organic content occur.

For CSH1, thermal degradation initiates with a ∼14% weight loss between 45 and 180 °C, slightly higher than that of native CS (∼6%), possibly due to increased hydrophilicity from grafted DMAPS and Am groups. The second stage of degradation, with (∼73%) weight loss, was observed between (∼260–475 °C). During this stage, the decomposition of side chains and the volatilization of gases such as CO_2, SO_2, NH_3, and CH_4.[9,46] Similarly, the ionic crosslinking of the copolymer with LSA, analogous to MBA crosslinking, results in a notable decrease in the thermal stability of pristine CS. Also, the thermal degradation of CSH2, CSH3, and CSH4 aerogels occurs in two distinct stages. The first stage, between 45 and 118 °C, corresponds to a ∼7% weight loss, primarily due to dehydration of adsorbed moisture and disruption of hydrogen bonding within the polymer network. The second stage spans 180–395 °C for CSH2 and CSH3, and extends to 410 °C for CSH4, with significant weight losses of 65, 68, and 72%, respectively. This phase is attributed to the decomposition of grafted polymeric side chains, pyrolysis of the CS backbone, and the release of volatile gases such as CH_4, CO_2, CO, and H_2S. Overall, grafting CS with DMAPS and Am reduced thermal stability. However, crosslinking with MBA slightly improved the thermal resistance of the resulting aerogels compared to those crosslinked with LSA.[50]

Surface morphology. Fig. 3a–d presents the scanning electron microscope images of CSH1, CSH2, CSH3, and CSH4. After CS grafting with poly(Am) and poly(DMAPS), the surface of CSH1 (Fig. 3a) shows large, smooth cross-linked sheets due to hydrogen bonding and ionic interactions between poly(DMAPS) *via* its SO_3^- groups and the NH_3^+ groups of CS. This crosslinking creates a high macroporous network. Fig. 3b and c showed thicker, tangled strands with smaller pores than in CSH1, yielding a tighter network (CSH2 and CSH3). The copolymers' surfaces have a rough, fine fibrillar appearance, indicating successful grafting of quaternary ammonium methacrylate onto CS dense cross-linking with LSA. This appearance is attributed to strong electrostatic interactions and intermolecular hydrogen bonds between LSA and the CS-grafted copolymer. Fig. 3d reveals a compact matrix with numerous uniforms, round micropores (1–5 μm) and hierarchical microporosity, providing abundant active sites for microbial neutralization. LSA (resulting in CSH2) led to a marked evolution into a well-organized, porous network; the average pore diameters were observed to range between 5 and 29 μm. When MBA was employed as a chemical crosslinker, the average pore diameter was observed to range from 6 to 33 μm for CSH4.[51]

Zeta potential (ζ) measurement. The net charge of CS and as-prepared CS copolymers was measured at pH 7.2 using dynamic light scattering (DLS) (Table 2). The average ζ of CS was found to be (−27.11 mV) due to deprotonation of the primary amine groups. By grafting CS with poly(Am) and poly(DMAPS), the ζ of the resulting CSH1 copolymer elevates to +30.5 mV. This dramatic increase can be explained by the presence of the cationic quaternary ammonium groups on the grafted poly(-DMAPS) side chains, which do not deprotonate at neutral pH, unlike the primary amine groups of the CS backbone. Ionic crosslinking of the grafted copolymer by LSA results in a decrease in ζ to +27.30 and +15.35 mV, depending on the amount of LSA used for crosslinking. On the other hand, the use of MBA as a chemical crosslinker (CSH2) resulted in a dramatic drop in ζ to +10.43 mV compared to CSH1.

Antibacterial activity

Effect of concentration, contact time, and ζ of different aerogels on *E. coli* enumerations. *Escherichia coli* (*E. coli*) originates from faecal contamination and is the main indicator of water pollution.[52] The tested CS-derived aerogels exhibited different capacities to reduce the number of *E. coli* in the test media. The aerogels were tested across a concentration range (0, 500, 1000, 2000, 3000, and 4000 ppm) to assess their antibacterial efficacy (Fig. 4). The application of different cross-linkers significantly affected the pathogen-eradication performance of

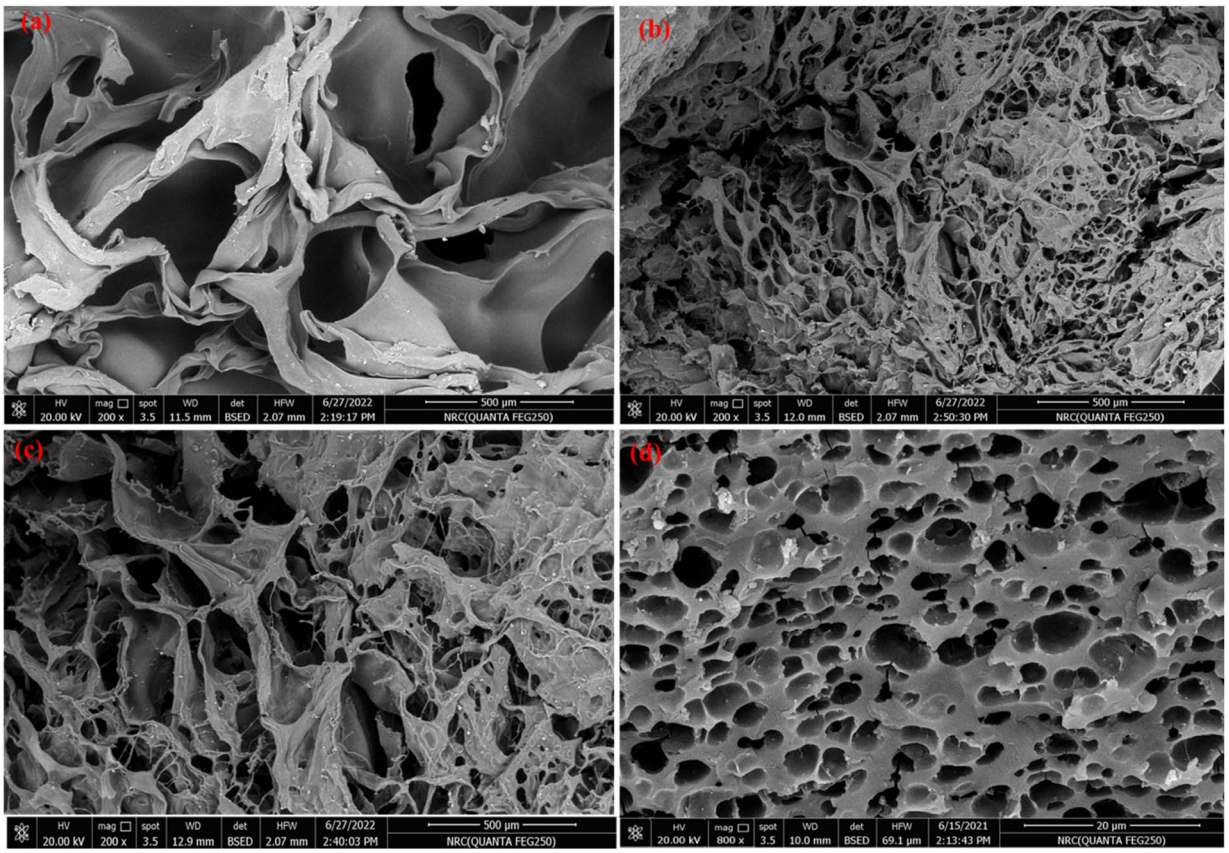

Fig. 3 SEM images for CSH1 (a), CSH2 (b), CSH3 (c), and CSH4 (d).

each aerogel. Among the tested formulations, CSH1 exhibited the highest antibacterial activity, achieving complete removal of *E. coli* at 2000 ppm within both 4 and 24 h. However, crosslinking CSH1 with LSA (CSH2) or MBA (CSH4) resulted in a remarkable change in the antibacterial activity.

Notably, the use of LSA as a crosslinker (CSH2 and CSH3) enhanced the antimicrobial performance compared with MBA-crosslinked aerogels (CSH4). A marked improvement in *E. coli* eradication was observed for CSH2, which had a lower LSA than CSH3 (Table 1). CSH2 demonstrated significant bacterial reduction at 500 ppm and achieved complete growth inhibition at 2000 ppm within 4 h. In contrast, CSH3 showed a gradual decline in *E. coli* counts with increasing aerogel concentration. The MBA-crosslinked aerogel (CSH4) exhibited the least antimicrobial efficacy, even at higher dosages. CSH1 exhibited the strongest ability to reduce *E. coli* counts among all tested aerogels, with complete inhibition of bacterial growth at 2000 ppm after both 4 and 24 h, confirming its potent bactericidal activity. This effect can be attributed to CSH1's capacity to diffuse through the bacterial cell wall and to interfere with intracellular proteins and ionic homeostasis, ultimately leading to cell disruption. In addition, the high cationic surface charge of CSH1 (30.50 mV) facilitates strong electrostatic interactions with the negatively charged bacterial membrane, promoting membrane destabilization and cell rupture.

Meanwhile, CSH2 showed a greater reduction in *E. coli* counts at 500 ppm, achieving complete eradication at 2000 ppm after 4 h. This concentration-dependent antimicrobial effect can be attributed to the cationic nature of CSH2, which exhibits a zeta potential of (+27.34 mV).[53] The high positive charge promotes strong electrostatic adhesion between the polymer surface and the negatively charged bacterial membrane, facilitating bacterial immobilization and subsequent inactivation.[30] In addition, the presence of an optimal amount of LSA as a crosslinker enhances the bactericidal performance of the aerogel, as LSA is a polyphenolic compound with intrinsic antimicrobial activity against both Gram-positive and Gram-negative bacteria.[44]

However, doubling the LSA amount led to a noticeable decline in antimicrobial efficacy, as evidenced by higher *E. coli* counts in CSH3. This reduction can be explained by the decreased cationic charge of CSH3 (+15.3 mV), which weakens

Table 2 ζ measured by DLS for CS, CSH1, CSH2, CSH3, and CSH4 at pH 7.2

Aerogel	CS	CSH1	CSH2	CSH3	CSH4
Zeta potential (ζ, mV)	−27.11 ± 0.4	+30.52 ± 0.28	+27.30 ± 0.87	+15.35 ± 0.05	+10.43 ± 0.54

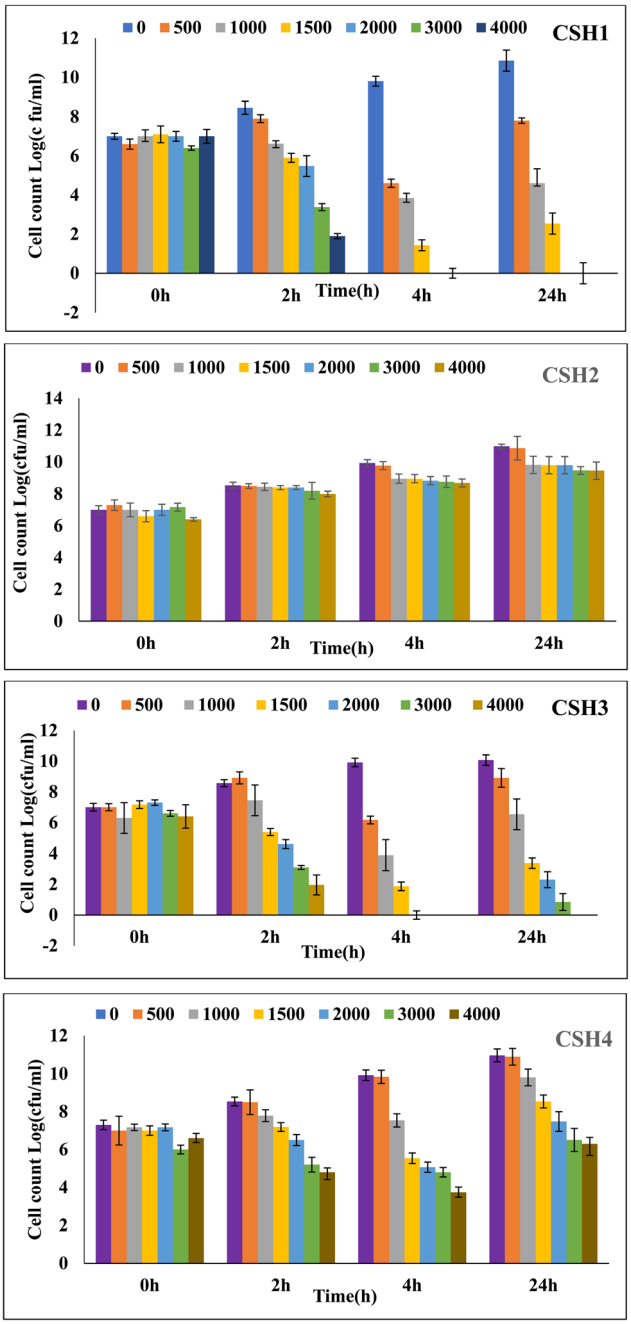

Fig. 4 Effect of concentration and contact time for the different aerogels on the bacterial cell count CSH1, CSH2, CSH3, and CSH4. Bar indicates ± standard deviation.

electrostatic interactions with bacterial cells. These findings strongly suggest that DMAPS is the primary contributor to the aerogels' antimicrobial activity, while the type and amount of crosslinker play a critical role in modulating their performance against *E. coli*. This observation is consistent with the report by Pérez-Aguilar *et al.*, who demonstrated that lignin exhibits lower antimicrobial activity against *Escherichia coli* (Gram-negative) compared with *Staphylococcus aureus* (Gram-positive).[40] The low ζ of CH4 against *E. coli* can be attributed to its low cationic charge at the neutral pH of the media, as confirmed by the measurement of aerogel ζ at pH 7.2, which mimics the pH of the growth media (10.43 mV).

The antimicrobial performance of the aerogels correlated strongly with their ζ and crosslinking density. Aerogels with higher positive surface charge (CSH1 and CSH2) exhibited stronger electrostatic attraction toward the negatively charged *E. coli* membrane, facilitating closer contact and more effective cell disruption. In contrast, CSH3, which contained a higher dosage of LSA, showed a markedly reduced zeta potential. Although charge weakening contributes to its diminished activity, the reduced efficacy cannot be attributed to surface charge alone. Excess LSA increases ionic crosslinking density, resulting in a more compact network with lower porosity and restricted diffusion of bacterial cells into the aerogel matrix. Furthermore, the bulky sulfonated aromatic groups of LSA can sterically shield CS's cationic sites, limiting their accessibility for membrane interaction.[54] The tighter network also reduces polymer chain mobility, which is essential for conformational adaptation during bacterial binding. Collectively, these structural effects explain why CSH3 exhibits lower antimicrobial potency despite being chemically similar to the more active formulations.[55,56]

The hundred-fold increase between the 4 and 24 h time points in the tested media may be due to most of the added polymers becoming attached to bacteria or other media components within the first 4 h, and most of the applied polymers becoming sequestered in the precipitated sediments or attached to bacterial cells. Bacteria that were still unaffected by the polymers reproduced rapidly over the remaining 20 h of the experiment Liu *et al.* (2016).[35]

The study of the mechanisms of CSH1 and CSH2 aerogels indicated that increasing the enumeration of *E. coli* about 3 times greater after mixing in case of CSH2 and these results supported the hypothesis that CSH2 can capture bacteria that can then be disrupted by vigorous mixing and this result explained the presence of *E. coli* numbers after 24 h of growth on nutrient broth media, although undetectable growth after 4 h in case of CSH2. Undetectable increase of *E. coli* counts after mixing for CSH1 may be due to cell death.

Mechanistic insights into the antibacterial action of chitosan-based aerogels by TEM. TEM imaging revealed distinct interaction mechanisms between CSH1 and CSH2 with *E. coli* cells (Fig. 5). TEM micrographs of CSH1 (Fig. 5b and c) showed that the aerogel diffused into bacterial cells, leading to membrane disruption and eventual cellular rupture, an effect attributed to its higher aqueous solubility. In contrast, TEM images of CSH2 (Fig. 5d–f) showed that *E. coli* cells adhered strongly to the aerogel surface, forming a dense coating in which the aerogel layer enveloped the bacterial cells. This interaction also induced noticeable flocculation, indicating that CSH2 promotes bacterial aggregation and immobilization primarily through surface binding rather than intracellular penetration.[57]

Applications of CSH2 aerogel in wastewater decontamination. The aqueous stability of CSH2, together with its strong eradication capability against *E. coli*, supported its selection for wastewater treatment applications. Wastewater was collected

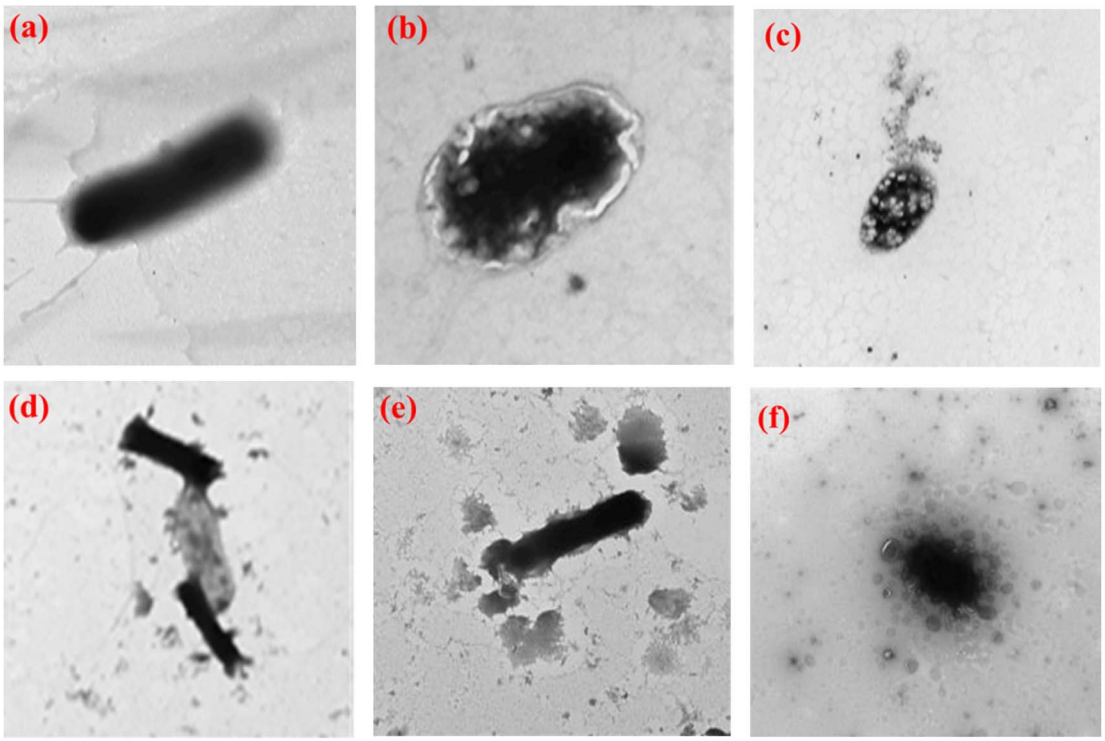

Fig. 5 TEM images for (a) bacterial cell without treatment, (b) and (c) *E. coli* after treatment with CSH1, and (d)–(f) *E. coli* after treatment with CSH2.

from the Belbies Drain in Sharqia Governorate, Egypt, and treated with different concentrations of CSH2 (1000, 2000, 3000, and 4000 ppm) to assess its decontamination efficiency (Table 3). Microbiological analysis of the untreated sample revealed high pathogen loads, including total coliforms (1.7×10^7 cfu mL^{-1}), faecal coliforms (4.2×10^5 cfu mL^{-1}), *Salmonella* (8×10^3 cfu mL^{-1}), and *Shigella* (3×10^4 cfu mL^{-1}). Treatment with 3000 ppm of CSH2 reduced faecal coliforms to below 10 cfu mL^{-1} and total coliforms to less than 100 cfu mL^{-1}, meeting the World Health Organization (WHO) criteria for safe water.[57,58] In addition, CSH2 exhibited excellent disinfection ability towards *Salmonella* at 2000 ppm and *Shigella* at 3000 ppm, respectively.

Physicochemical characterization of a wastewater sample. The removal of suspended solids and colloidal matter is essential for effective decontamination of the wastewater sample. Physicochemical measurements of water, such as pH, BOD, COD, and turbidity, are essential for maintaining water quality and ensuring compliance with environmental regulations. Treatment of the sample with CSH2 at 3000 ppm significantly improved its physicochemical quality. The levels of BOD, COD, and TOC were reduced to values compliant with the limits specified by Egyptian Law 92 (0.00, <50, and <3, respectively), as shown in Table 4. In addition, CSH2 demonstrated excellent clarification performance, reducing turbidity from 18 NTU to <1 NTU (0.2 NTU), meeting the USEPA (2009) and World Health Organization (WHO, 1989) turbidity standards. The treatment also demonstrated strong potential to eliminate unpleasant odors, further supporting CSH2's suitability for wastewater purification applications. The efficacy of CSH2 in removing the majority of these compounds is predominantly achieved *via* coagulation and flocculation. The physicochemical principle behind coagulation is the reduction of the repulsive electrical potential between typically electronegative colloidal particles in water, such as color, NOM, microorganisms, clays, *etc.*, in such

Table 3 Effect of CSH2 on the decontamination of different wastewater pathogens

CSH2 conc. (ppm)	Total coliform (cfu ml^{-1})	Faecal coliform (cfu ml^{-1})	*Salmonella* (cfu ml^{-1})	*Sheigella* (cfu ml^{-1})
0	17×10^6	42×10^4	8×10^3	3×10^4
1000	83×10^4	3×10^3	5×10^2	7×10^2
2000	58×10^2	98	ND	53
3000	91	7	ND	ND
4000	ND	ND	ND	ND

Table 4 Physicochemical parameter analysis in a low-quality water sample

Parameter	Before treatment	After treatment	Law (92)
Temperature (°C)	29	29	>3
Turbidity (NTU)	18	0.2	—
BOD (mg L^{-1})	60	—	—
COD (mg L^{-1})	91	6	<50
TOC (mg L^{-1})	14	1	<3
Odor	Unpleasant odor	—	—

a way that the coagulant causes these suspended, dispersed particles to destabilize and agglomerate to form large, dense structures (flocs) that will precipitate and sediment.[59] It should be noted that the microbial counts and the physicochemical characterization for the waste water sample reflect conditions immediately after treatment, and the long-term stability of the treated water was not monitored; therefore, the potential for recontamination during storage remains an important consideration for future evaluation.

Moreover, CS biopolymers are well known as bioactive coagulants and have achieved colloids removal by different mechanisms, including a combination of physical–chemical processes, such as charge neutralization, adsorption, formation of complexes with metals, and precipitation.[60,61]

The comparison of performance of our dual–crosslinked zwitterionic chitosan–lignosulfonate aerogel (CSH2) in nutrient broth and real wastewater highlights both its intrinsic antimicrobial potency and its robustness under environmentally relevant conditions. In nutrient broth, CSH2 achieved complete eradication of *E. coli* at 2000 ppm within 4 h, demonstrating strong activity in a controlled medium with minimal competing organic load. When applied to real wastewater characterized by suspended solids, high organic content, and a diverse microbial community CSH2 maintained high efficacy, reducing total coliforms, fecal coliforms, *Salmonella*, and *Shigella* to WHO-compliant levels. This performance compares favorably with previously reported chitosan-based hydrogels (Table 5) polysaccharide aerogels, and lignin-modified antimicrobial materials, many of which exhibit reduced activity in real wastewater due to charge shielding, competitive adsorption, or structural instability. In contrast, the combined covalent/ionic crosslinking strategy in CSH2 provides enhanced aqueous stability and sustained surface–adhesive interactions, enabling consistent antimicrobial action across both simplified and highly heterogeneous matrices. Collectively, these findings position CSH2 among the more effective bio-derived antimicrobial aerogels reported to date, offering a competitive and field-relevant solution for pathogen mitigation in wastewater.

Limitations and future work

• Although the synthesized chitosan-derived aerogels demonstrated strong antibacterial activity against *E. coli* and performed effectively in real wastewater, the antimicrobial evaluation in this study focused on a single Gram-negative model organism. Future research will therefore focus on expanding the antimicrobial assessment to include a broader range of pathogenic microorganisms.

• Additionally, the long-term stability, regeneration capacity, and multi-cycle reusability of the aerogels were not investigated. Future work will investigate the aerogels' long-term operational stability, structural integrity, and antimicrobial efficiency over repeated treatment cycles to determine their reusability and practical lifespan. Besides, the aerogel performance under varying environmental or storage conditions will be evaluated. To determine their practical applicability in large-scale wastewater treatment systems.

• Mechanistic studies such as charge-density measurements, membrane integrity assays, reactive oxygen species quantification, and molecular interaction analyses will be conducted to establish a more rigorous mechanistic correlation and to strengthen the understanding of how surface charge governs the antimicrobial behavior of the developed aerogels.

Table 5 Comparative study for different previously reported chitosan-derived scaffolds for microbial decontamination for wastewater

Scaffold composition	Characteristic feature and action mode	Ref.
Carboxymethyl chitosan-*graft*-poly[(2-methacryloyloxyethyl) trimethylammonium chloride] copolymer	Exhibited a bactericidal effect against *E. coli* in the test medium	30
Chitosan-grafted poly(vinyl benzyl trimethylammonium chloride) semi-IPN hydrogels	Bactericidal effects against coliforms and *C. perfringens*, by 51.3% and 53%, respectively. *E. faecalis*, *S. typhimurium*, *L. pneumophila*, and *Shigella* spp., could be eliminated by the hydrogels	62
Cellulose filter papers-modified polydopamine, polyethylene-imine and ZnO/Ag/GO nanocomposite papers	Bactericidal effect against *E. coli* with (99.98%) bacterial reduction	
Polyvinyl chloride-grafted cationic methylimidazolium	Removal of *E. coli* (6 LRV) from wastewater	63
Imidazole cross-linked chitosan/PEI hydrogel and enriched with inorganic salt	Orange and metanil yellow dyes removal. Antibacterial activity against *E. coli* and *S. aureus*	64
Poly(2-methacryloxyethyl phosphorylcholine)-grafted chitosan	~87.7% inhibition against *E. coli*, due to zwitterionic PMPC's antifouling behavior and chitosan's antibacterial functionality	65
Zweiteric chitosan–lignosulfonate derived aerogel	Achieved complete eradication of *E. coli* from nutrient medium at 2000 ppm within 4 h	
In a wastewater sample at 3000 ppm reduced faecal coliforms to below 10 cfu mL^{-1}, and total coliforms to less than 100 cfu mL^{-1}	Our work	

• Finally, scaling-up strategies, cost-effectiveness assessments, and pilot-scale field trials will be pursued to support the translation of the most promising aerogel formulations, particularly CSH2, into practical wastewater treatment technologies.

Conclusion

This study demonstrates the promising potential of the synthesized chitosan-based aerogels as effective antimicrobial and wastewater-treatment materials. CSH1 exhibited the highest bactericidal activity against *E. coli*, driven by its strong cationic charge and ability to penetrate bacterial cells, leading to membrane disruption and intracellular damage. In contrast, CSH2 operated through a distinct mechanism, promoting strong surface adhesion, aggregation, and bacterial cell immobilization, as confirmed by TEM imaging. The presence and optimal amount of LSA as a crosslinker further enhanced the antimicrobial performance of CSH2, while excessive LSA reduced activity due to diminished surface charge. Beyond antimicrobial efficacy, CSH2 demonstrated significant improvements in the physicochemical quality of real wastewater samples. Treatment at 3000 ppm significantly reduced BOD, COD, TOC, turbidity, and pathogenic bacterial loads to levels compliant with national and international water-quality standards. These combined results highlight the multifunctional capability of chitosan-based aerogels, emphasizing their potential as sustainable, efficient, and environmentally friendly materials for water purification and microbial control applications.

Although the synthesized chitosan-based aerogels demonstrated strong antimicrobial activity and excellent performance in wastewater treatment, several limitations should be acknowledged. First, the antimicrobial evaluation focused primarily on *E. coli* as a representative Gram-negative bacterium. Additional studies involving a broader panel of Gram-positive and Gram-negative pathogens, as well as antibiotic-resistant strains, are necessary to fully establish the spectrum and robustness of antimicrobial activity. Moreover, while TEM imaging provided valuable mechanistic insights, complementary techniques such as AFM force measurements and proteomic analysis of treated cells could further clarify the interaction pathways of CSH1 and CSH2. For wastewater treatment, the experiments were conducted under controlled laboratory conditions using real wastewater samples. However, long-term performance under variable environmental conditions such as fluctuating pH, ionic strength, organic load, and microbial diversity remains to be evaluated. The regeneration, reusability, and mechanical stability of the aerogels during repeated treatment cycles also require systematic investigation to assess their economic feasibility for large-scale deployment.

While the current study focused on optimizing the aerogel formulation to balance antimicrobial potency and structural stability. Future work will focus on multi-cycle reusability and aerogel stability studies, scaling-up strategy, including pilot-scale column filtration or batch treatment systems, to provide critical insights into industrial applicability. Cost-benefit analysis will be essential to position these chitosan-based aerogels as viable, eco-friendly alternatives for integrated water purification and microbial control technologies.

Ethical statement

The study utilized only identified laboratory bacterial strains and did not involve vertebrate animals or human participants. The microbiology assays were conducted in accordance with the protocols approved by the local ethical committee (Ethical Committee of the National Research Centre). In accordance with national and institutional policies governing non-animal microbiological research, no animal use or human subject ethical approval was required.

Author contributions

Naglaa Salem El-Sayed and Samir Kamel proposed the work plan. Naglaa Salem El-Sayed performed the chemical synthesis and material characterization. Doaa Ali performed the antimicrobial studies. All authors contributed equally to writing the manuscript. All authors have approved the final version of the manuscript.

Conflicts of interest

The authors declare that they have no known competing financial interests or personal relationships that could have influenced the work reported in this paper.

Data availability

The data that support the findings of this study are available from the authors upon reasonable request.

Acknowledgements

The authors thank the National Research Centre, Egypt, for the facilities support.

References

1 C. P. Jiménez-Gómez and J. A. Cecilia, *Molecules*, 2020, **25**, 3981.
2 A. Al-Sayed, G. K. Hassan, M. T. Al-Shemy and F. A. El-Gohary, *Sci. Rep.*, 2023, **13**, 15601.
3 G. K. Hassan, M. Al-Shemy, A. M. Adel and A. Al-Sayed, *Sci. Rep.*, 2022, **12**, 19666.
4 N. M. Ali, M. K. Khan, B. Mazhar and M. Mustafa, *Discover Water*, 2025, **5**, 19.
5 A. R. Salem, W. A. Kassab, A. M. Adel, M. El-Sakhawy and M. T. Al-Shemy, *Process Saf. Environ. Prot.*, 2025, **197**, 106985.
6 Y. Chen, H. Xu, M. S. Khan, S. Han and S. Zhu, *Crit. Rev. Environ. Sci. Technol.*, 2025, **55**, 1097–1123.
7 N. A. Oladoja, E. I. Unuabonah, O. S. Amuda and O. M. Kolawole, *Polysaccharides as a green and sustainable resources for water and wastewater treatment*, Springer, 2017.

8 X. Qi, X. Tong, W. Pan, Q. Zeng, S. You and J. Shen, *J. Clean. Prod.*, 2021, **315**, 128221.
9 K. H. Kamal, M. A. Hassan, S. Kamel and N. S. El-Sayed, *Surf. Interfaces*, 2024, **51**, 104596.
10 N. S. EL-Sayed, S. Dacrory, M. El-Sakhawy, E. B. Hassan and S. Kamel, *Adsorption*, 2025, **31**, 1–15.
11 N. S. El-Sayed, K. H. Kamal, M. El-Sakhawy, E. B. Hassan and S. Kamel, *J. Water Process Eng.*, 2025, **72**, 107478.
12 S. Zhu, M. S. Khan, K. Xiao, C.-M. Chang, Q. Zhao, T.-S. Chung and S. B. Chen, *J. Membr. Sci.*, 2026, **744**, 125198.
13 N. S. El-Sayed, A. N. Shirazi, M. G. El-Meligy, A. K. El-Ziaty, Z. A. Nagieb, K. Parang and R. K. Tiwari, *Int. J. Biol. Macromol.*, 2016, **87**, 611–622.
14 N. S. El-Sayed, M. Sharma, H. M. Aliabadi, M. G. El-Meligy, A. K. El-Zaity, Z. A. Nageib and R. K. Tiwari, *Int. J. Biol. Macromol.*, 2018, **112**, 694–702.
15 C. K. Coleman, H. H. Oza, E. S. Bailey and M. D. Sobsey, *Environments*, 2024, **11**, 211.
16 G. Farinelli, H. Baldo, L. Soussan, F. Lefèbvre, K. Sénéchal-David, J.-N. Rebilly, F. Banse and D. Quemener, *Water*, 2025, **17**, 3077.
17 M. A. Shehab, M. Al-Lami, M. A. Taher, H. H. Mohammed, A. A. AbdulRazak, K. T. Rashid, A. Mahmood, M. F. Abd Al-Ogaili and S. Alsarayefi, *RSC Adv.*, 2025, **15**, 29727–29742.
18 H. Abdelmegeed, N. M. Helmy, A. M. A. Hassan, M. S. Abdel-aziz, A. K. Elziaty, S. Kamel, Z. Li, Q. Wang and N. S. El-Sayed, *Int. J. Biol. Macromol.*, 2026, **362**, 152083.
19 M. Yan, W. Huang and Z. Li, *Int. J. Biol. Macromol.*, 2019, **136**, 927–935.
20 H. Lu, H. Zhu, J. Xu, X. Lai, X. Zeng and H. Li, *Chem. Eng. J.*, 2024, **497**, 154868.
21 S. Kamel and N. S. El-Sayed, in *Injectable Smart Hydrogels for Biomedical Applications*, ed. J. M. Dodda, N. Ashammakhi and E. R. Sadiku, Royal Society of Chemistry, 2024, vol. 17.
22 P. Dong, X. Shu, R. Peng, S. Lu, X. Xie and Q. Shi, *Mater. Sci. Eng., C*, 2021, **128**, 112327.
23 L. Li, H. Li, M. Lin, N. Wang, S. Hu and J. Wen, *Sep. Purif. Technol.*, 2024, **348**, 127695.
24 Y. Zhu, T. Zhang, L. Lv, W. Tang, Y. Wang and S. Tang, *Sep. Purif. Technol.*, 2025, **354**, 129272.
25 P. Sun, J. Jin, M. Wang, J. Ma and H. Wang, *ACS Appl. Mater. Interfaces*, 2025, **17**, 60126–60133.
26 G. Turky, M. A. Moussa, M. Hasanin, N. S. El-Sayed and S. Kamel, *Arabian J. Sci. Eng.*, 2021, **46**, 17–30.
27 N. S. El-Sayed, A. H. Hashem, T. A. Khattab and S. Kamel, *Int. J. Biol. Macromol.*, 2023, **248**, 125872.
28 M. Lazaridou, S. Nanaki, A. Zamboulis, C. Papoulia, K. Chrissafis, P. A. Klonos, A. Kyritsis, S. Vergkizi-Nikolakaki, M. Kostoglou and D. N. Bikiaris, *Int. J. Pharm.*, 2021, **606**, 120925.
29 N. Kaur Dhiman, S. Agnihotri and M. Sudhakara Reddy, *Chem. Eng. J.*, 2024, **489**, 151335.
30 Z. Yang, J.-R. Degorce-Dumas, H. Yang, E. Guibal, A. Li and R. Cheng, *Environ. Sci. Technol.*, 2014, **48**, 6867–6873.
31 X. Li, X. Zhang, S. Xie, Y. Ge, L. Feng and W. Li, *RSC Adv.*, 2022, **12**, 20857–20865.
32 X. Yang, W. Ban, R. Zhang, X. Li, M. Huang, Q. Yang and B. Yan, *Ind. Eng. Chem. Res.*, 2024, **63**, 2534–2543.
33 H. Luo, J. Zeng, M. Xu, Q. Tang, T. Liu, S. Wu, S. Li and H. Rong, *Int. J. Biol. Macromol.*, 2025, **289**, 138872.
34 R. M. Atlas, *Handbook of media for environmental microbiology*, CRC Press, 2005.
35 Z. Liu, Z. S. Carroll, S. C. Long, S. Gunasekaran and T. Runge, *J. Environ. Manag.*, 2016, **166**, 260–266.
36 J. Versalovic, *Manual of clinical microbiology*, American Society for Microbiology Press, 2011.
37 A. P. H. Association, *Standard methods for the examination of water and wastewater*, American Public Health Association, 1926.
38 N. Manivasakam, *Industrial Water Analysis Handbook*, Chemical Publishing, 2005.
39 P. Quinn, B. Markey, M. Carter, W. Donnelly and F. Leonard, *Anim. Welfare*, 2002, **11**, 138.
40 H. Pérez-Aguilar, V. M. Serrano-Martínez, M. P. Carbonell-Blasco, A. García-García and E. Orgilés-Calpena, *Biofuel Bioprod. Biorefining*, 2025, **19**, 1378–1399.
41 N. S. El-Sayed and S. A. Al Kiey, *J. Power Sources*, 2026, **676**, 239797.
42 E. Zong, C. Zhang, S. Wu, Y. Gao, J. Yang, X. Liu and P. Song, *Int. J. Biol. Macromol.*, 2023, **241**, 124511.
43 J. Hu, D. Zhang, W. Li, Y. Li, G. Shan, M. Zuo, Y. Song, Z. Wu, L. Ma and Q. Zheng, *ACS Appl. Mater. Interfaces*, 2024, **16**, 6433–6446.
44 N. S. El-Sayed, S. A. Al Kiey, A. Darwish, G. Turky and S. Kamel, *Int. J. Biol. Macromol.*, 2022, **218**, 420–430.
45 H. Mackova, Z. Plichta, H. Hlídková, O. Sedlacek, R. Konefal, Z. Sadakbayeva, M. Duskova-Smrckova, D. Horak and S. Kubinova, *ACS Appl. Mater. Interfaces*, 2017, **9**, 10544–10553.
46 F. Gu, J. Geng, M. Li, J. Chang and Y. Cui, *ACS Omega*, 2019, **4**, 21421–21430.
47 J. Zhang, Y. Yuan, J. Shen and S. Lin, *Eur. Polym. J.*, 2003, **39**, 847–850.
48 Q. Liu, L. Ji, W. Lin, Y. Sun, X. Lin, Y. Xie, J. Xie and G. Yi, *J. Polym. Res.*, 2025, **32**, 1–12.
49 S. Kumar and J. Koh, *Int. J. Mol. Sci.*, 2012, **13**, 6102–6116.
50 S. S. Saima Sohni, R. H. Rokiah Hashim, H. N. Hafiz Nidaullah, J. L. Junidah Lamaming and O. S. Othman Sulaiman, *Int. J. Biol. Macromol.*, 2019, **132**, 1304–1317.
51 S. S. Narasagoudr, V. G. Hegde, V. N. Vanjeri, R. B. Chougale and S. P. Masti, *Carbohydr. Polym.*, 2020, **236**, 116049.
52 P. Tallon, B. Magajna, C. Lofranco and K. T. Leung, *Water Air Soil Pollut.*, 2005, **166**, 139–166.
53 S. Zhu, Q. Zhao, Y. Chen, M. S. Khan, C.-M. Chang, T.-S. Chung and S. B. Chen, *Environ. Sci. Technol.*, 2026, **60**(2), 2160–2172.
54 C.-L. Ke, F.-S. Deng, C.-Y. Chuang and C.-H. Lin, *Polymers*, 2021, **13**, 904.
55 R. P. Pandey, K. Rasool, P. A. Rasheed, T. Gomez, M. Pasha, S. A. Mansour, O.-S. Lee and K. A. Mahmoud, *Green Chem.*, 2020, **22**, 678–687.
56 C. Xu, L. Liu, S. Renneckar and F. Jiang, *Ind. Crops Prod.*, 2021, **170**, 113759.

57 C. Ardean, C. M. Davidescu, N. S. Nemeș, A. Negrea, M. Ciopec, N. Duteanu, P. Negrea, D. Duda-Seiman and V. Musta, *Int. J. Biol. Macromol.*, 2021, **22**, 7449.
58 W. H. Organization, *Yersinia enterocolitica: background document for the WHO guidelines for drinking-water quality and the WHO guidelines on sanitation and health*, World Health Organization, 2025.
59 S. D. Faust and O. M. Aly, *Chemistry of water treatment*, CRC Press, 2018.
60 M. Khajavian, S. Ismail and V. Vatanpour, *Adv. Eng. Mater.*, 2026, e202502390.
61 S. Jain and A. Khanna, *ChemistrySelect*, 2026, **11**, e05462.
62 I. E. Neblea, A.-L. Chiriac, A. Zaharia, A. Sarbu, M. Teodorescu, A. Miron, L. Paruch, A. M. Paruch, A. G. Olaru and T.-V. Iordache, *Polymers*, 2023, **15**, 1091.
63 D. Shen, H. Ma, M. Khan and B. S. Hsiao, *Chem. Eng. J.*, 2024, **479**, 147269.
64 Y. Li, L. Xie, J. Liu, S. Tang, H. Lei, Y. Zhong and Y.-F. Zhang, *Int. J. Biol. Macromol.*, 2025, **309**, 142904.
65 C. G. Alves, D. de Melo-Diogo, R. Lima-Sousa and I. J. Correia, *Int. J. Pharm.*, 2020, **582**, 119346.